RSC Advances

ROYAL SOCIETY OF CHEMISTRY

www.rsc.org/advances

Graphic for

A sustainable iron-based sodium ion battery of porous carbon-Fe_3O_4/$Na_2FeP_2O_7$ with high performance

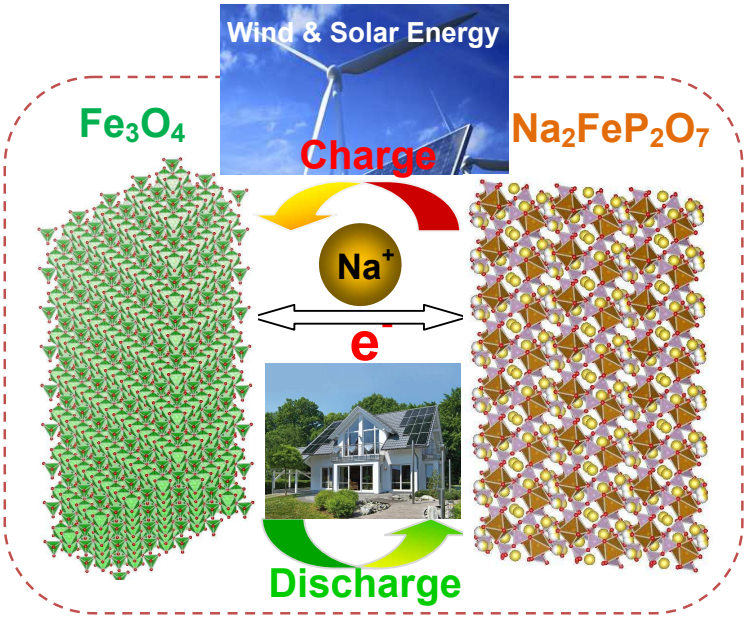

A new concept of elemental iron-based sodium ion battery of PC-Fe_3O_4/$Na_2FeP_2O_7$ was reported, and it is the first example to introduce an element-rich configuration in sodium ion battery from the viewpoint of sustainability.

Journal Name

RSCPublishing

ARTICLE

A sustainable iron-based sodium ion battery of porous carbon-Fe_3O_4/$Na_2FeP_2O_7$ with high performance

Cite this: DOI: 10.1039/x0xx00000x

Received 00th January 2012,
Accepted 00th January 2012

DOI: 10.1039/x0xx00000x

www.rsc.org/

Jun Ming,[†a] Hai Ming,[†b] Wenjing Yang,[c] Won-Jin Kwak,[a] Jin-Bum Park,[a] Junwei Zheng,[b] Yang-Kook Sun[a]*

One kind of porous carbon-Fe_3O_4 (*e.g.*, PC-Fe_3O_4) composite with an industrial production was introduced in the sodium ion battery application for the first time. The PC-Fe_3O_4 composite, consisting of highly dispersed Fe_3O_4 nanocrystals within the porous carbon with a relative low percent of 45.5 wt%, could well demonstrate high capacities of 225, 168, 127, 103, 98 and 90 $mAhg^{-1}$ under the current densities of 50, 100, 200, 300, 400 and 500 mA g^{-1} with a good stability over 400 cycles. The utilization co-efficient of Fe_3O_4 nanocrystals was proved to be much higher than most Fe_3O_4 nanoparticles reported recently under the study of capacity contribution of carbon originally. And also, the robust of electrode during the charge-discharge was well characterized by the ex-situ XRD and emission scanning electron microscopy (SEM). More importantly, a new concept of elemental iron-based sodium ion battery of PC-Fe_3O_4/$Na_2FeP_2O_7$ was presented. This is the first example to introduce an element-rich configuration in sodium ion battery from the viewpoint of sustainability. The full battery demonstrated a superior capacity of 93 mAh g^{-1}, high capacity retention of 93.3% over 100 cycles and work voltage around 2.28 V with the energy density of 203 Wh kg^{-1}. Such configuration of iron-based sodium battery would be highly promising and sustainable owing to its low cost and high stability in grid storage.

Introduction

The development of cost-effective battery with a high safety is a great challenge to promise the large-scalable application of lithium and sodium batteries in electronic vehicle (EV) and grid storage.[1-3] Especially with the strong tendency of abundant sodium ion battery instead of the source/cost-limited lithium one, the safety issue becomes ever more important due to the higher burning activity of sodium metal exposed to oxygen or moisture.[4] Considering these aspects, configuration of ideal sodium ion battery system, particularly based on developing appropriate anode and cathode, are very significant to ensure its sustainability and safety.

To develop the anode, a popular research trend of preparing various carbon and/or metal (oxide) based materials appeared recently under the similar way as those in lithium ion battery.[5-9] The carbon and metal oxide-based materials with different morphologies, structures and compositions are being widely synthesized, such as carbon fiber,[10] hollow carbon tubes,[11] graphene,[12] Sn-SnS-C,[13] Fe_2O_3-graphene,[14] CuO arrays,[15] TiO_2[16] and TiO_2-C.[17] Indeed, most of them demonstrated excellent performance due to the intriguing properties of nano-characteristics. However, the aspects of cost and safety of materials, as well as the synthetic process should be well considered for their practical commercialization. To improve the safety, more and more researchers prefer to develop metal oxide-based anode instead of carbon because of their great advantages of high capacity, non-flammable ability and low voltage around 0.7-0.9 V which could effectively suppress the deposition of metal dendrite.[18] But inevitably, most processes always spend a high cost and need complex procedures for the manipulation. Naturally, it would be great to get the nano-structured materials with a high performance via a simple approach, particularly with using low-cost element abundant in the earth. Therefore herein, we introduced one new composite of iron oxide-based anode of porous carbon-Fe_3O_4 in sodium ion battery for the first time, which could be obtained in an industrial scalable way, rather than the experimental amount of Fe_3O_4 particles obtained by the hydrothermal method.[19-21] It is well known that the iron was the fourth highest element in the earth only less than O, Si and Al. The high content of 5.1wt%, together with the physicochemical characteristics of highly non-flammable and suitable voltage around 0.7-0.9 V, could

make the iron oxide-based anode to be a very competitive anode in battery for sustainability.

Although the sodium ion battery has been attracting great attention recently both in anode and cathode (e.g., P2-type $Na_x[Fe_{1/2}Mn_{1/2}]O_2$,[22] $Na_x[Ni_{1/3}Mn_{2/3}]O_2$,[23] $Na_3V_2(PO_4)_2F_3$,[24] $Na_2FeP_2O_7$[25,26]), however, the cases of developing a full battery were very limited,[27] especially further concerning the matters of safety and cost. Undoubtedly, it would be very interesting and significant to develop full batteries to evaluate their combined performance as those in practical applications, and it should be a big step towards commercialization improved from the isolated researches on anode or cathode. To accelerate these materials available and be utilized in practical application, herein we introduced a new concept of elemental iron-based sodium battery of PC-Fe_3O_4/$Na_2FeP_2O_7$, in which the safe and cost-effective electrode of $Na_2FeP_2O_7$ and PC-Fe_3O_4 were chosen. It is the first example to introduce an element-rich configuration in sodium ion battery from the viewpoint of sustainability. The designed battery demonstrated a high capacity of 93 mAh g^{-1} at 0.1 C, cycle ability over 100 cycle with a capacity retention of 93.3% at 0.1 C, work voltage around 2.28 V with a energy density of 203 Wh kg^{-1}. In theory, such configuration of elemental iron-based battery was highly promising and sustainable for its low cost and high safety.

Experimental

Anode preparation

The 15.0 g Pluronic F127 was dissolved in 60 g of ethanol at 40 °C firstly, and then 25 g $Fe(NO_3)_3{\cdot}9H_2O$ and 45 g of resol-ethanol (20 wt %) were added into the solution successively. After stirring for 4 h, the solution was then transferred into the oven and dried it at a high temperature of 100 ^oC. The heating rate of temperature should be controlled slowly till to the final 100 ^oC for avoiding any mild explosion of solution. The dried sample was calcined at 500 ^oC (heating rate, 2 ^oC min^{-1}) for 2 h in the furnace under the Ar flow. Without adding the precursors of $Fe(NO_3)_3{\cdot}9H_2O$ into the solution, porous carbon could be obtained under the same procedures. The compared Fe_3O_4 particles were prepared based on the previous procedures.[28, 29] Typically, 27g $FeCl_3{\cdot}6H_2O$ was dissolved in 800 ml ethylene glycol to form a clear solution, and then adding 72 g NaAc and 20 g polyethylene glycol (PEG-400) into the solution successively. The mixture was stirred vigorously for 30 min and then sealed in a 1000 ml Teflon lined stainless-steel autoclave. The autoclave was heated to and maintained at 200 ^oC for 8 h, and then cooling down to the room temperature naturally. Wash the Fe_3O_4 particles with using the water and ethanol several times under stirring. Noteworthy, the samples could be collected effectively by the magnetic after each procedure of wash, rather than any separation or centrifugation.

Cathode preparation

The material of $Na_2FeP_2O_7$ was synthesized via a solid state reaction, in which the stoichiometric amounts of Na_2CO_3, $(NH_4)_2HPO_4$ and $FeC_2O_4{\cdot}2H_2O$ were ball milling firstly.[30] And then the powder was pelletized and pre-heated at 350 ^oC for 3 h in an argon atmosphere. The pellet was reground into powders and then re-pelletized for the re-calcination at 600 ^oC for 6 h in Ar. Finally, the obtained $Na_2FeP_2O_7$ was further coated by the carbon based on the following procedures. Ball milling the powders of $Na_2FeP_2O_7$ and acetylene black (AB) with the mass ratios of 8/2, and then calcination of pressed pellet at 600 ^oC for 10 h under Ar flow, finally giving rise to carbon modified $Na_2FeP_2O_7$.

Electrode Preparation

The anode of PC-Fe_3O_4, the binder of CMC/PAA rather than polyvinylidene difluoride (PVDF), and conductive carbon of AB with the mass ratio of 80:10:10 were mixed in the solvent of water to form homogeneous slurry. And then, the slurry was casted on the copper foil by the doctor blade. Keep at room temperature first for almost dry and then transfer to vacuum oven at 80 ^oC over night. Punch the foil to circular electrode with the diameter of 16 mm. The mass density of PC-Fe_3O_4 in the electrode was about 1.5 mg cm^{-2}. Alternatively, the powders of electrode, obtained from vacuum-drying the aqueous slurry of PC-Fe_3O_4-CMC/PAA-AB, was pressed into tablet (Ø14 mm) for the characterization of ex-situ XRD with the aim of avoiding the interference of copper foil. The reason of selecting the binder of CMC/PAA and the green solvent of water were ascribed to the better performance in lithium and sodium ion battery applications as reported recently.[31] For the preparation of cathode, the composite of $Na_2FeP_2O_7$-AB, binder of PVDF, conductive carbon of AB, were mixed well in the mass ratio of 85:10:5 to form the slurry, and then it was casted on the Al foil. Dry at 120 ^oC in vacuum oven overnight and then punch it into circular electrode before use. The mass density of $Na_2FeP_2O_7$ in the electrode keeps around 3.48 mg cm^{-2}.

Characterization

The morphology and structure of PC-Fe_3O_4 and electrode were characterized by field emission scanning electron microscopy (FESEM), which was taken on a XL30 ESEM microscope with beam energy of 20 kV. The encapsulated Fe_3O_4 nanocrystals were characterized by the transmission electron microscopy (TEM) images using a JEOL-2100F microscope operated at 200 kV. Crystallographic information of PC-Fe_3O_4 and electrode were investigated by XRD, which were measured on a Brucker D8 GADDS diffractometer using Co Ka radiation (1.79 Å). For the cycled electrode disassembled from the coin cell, they were protected by the cover from contacting air. The Fe valences were determined by using XPS, and the spectrum was recorded on an ESCALAB 250 spectrometer. The monochromatized AlKa X-ray source for the XPS was operated at 12 kV and 20 mA.[32] The surface area and porosity of PC-Fe_3O_4 and porous carbon were determined by using a Quantachrome Autosorb-1-MP automated gas adsorption system using nitrogen as the adsorbate at liquid nitrogen temperature (77 K). The samples were out gassed under vacuum for 24 h at 100 ^oC. The specific surface area was calculated using the Brunauer-Emmett-Teller (BET) method,

and the porous characteristic was determined using the t-plot method. The mass content of Fe_3O_4 was measured by the thermalgravimetric analysis (TGA, 10 ^oC min^{-1}, Air). The 2032-type coin cells were assembled in the glove box in which the water and oxygen content are both below 0.1 ppm. In the battery test, the electrolyte was 1.0 M $NaClO_4$ in propylene Carbonate (PC) with 2vol.% fluoroethylene carbonate (FEC), and the glass fibre was used as the separator. The battery of PC-Fe_3O_4/Na and PC-Fe_3O_4/$Na_2FeP_2O_7$ were performed within the voltage of 0.01-3 V and 1.1-4.2 V respectively with using the instrument of *TOCAST* 3100 at the temperature of 30 ^oC. The cyclic voltammetry (CV) of Fe_3O_4/Na within the voltage of 0.01-3.0 V was analyzed using the VMP-3 instrument.

Results and discussion

The hierarchical structure of PC-Fe_3O_4 composite, consisting of encapsulated Fe_3O_4 nanocrystals around the size of 10-15 nm within the porous carbon, could be clearly observed and confirmed by the SEM, TEM and HRTEM (Fig. 1a-c, marked by yellow circle). The exposed lattice distance of 2.518 Å well correspond to the Fe_3O_4 planes of (311) (Fig. 1c). Besides, the indexed diffraction patterns of (002), (311), (004), (333) and (044) in selected area electron diffraction (SAED) were in good accordance with the XRD result, as shown in Figure 2a. Except the pattern of (422), which was too weak to observe in SAED and also not obvious in XRD (Fig. 1d, Fig. 2a). The crystal structure of Fe_3O_4 belongs to the space group of FD-3MZ (ICSD#633020),[33] in which the octahedral FeO_6 were corner connected by bridged O and the cell parameters of a, b and c were 8.3528 Å, as characterized by the Rietveld results of XRD pattern (Fig. 2b).[34] The main visual structure of PC-Fe_3O_4 was shown in Figure 1d, in which the Fe_3O_4 nanocrystals were

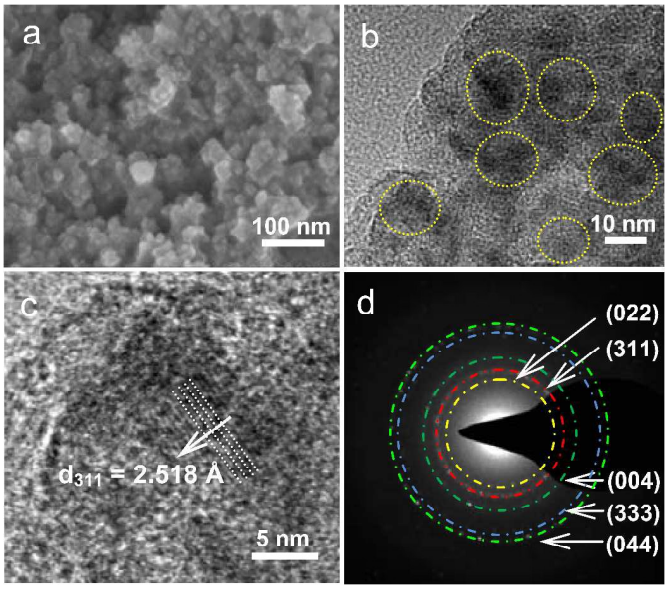

Figure 1 (a) SEM, (b) TEM, (c) HRTEM and (d) SAED of PC-Fe_3O_4 composite.

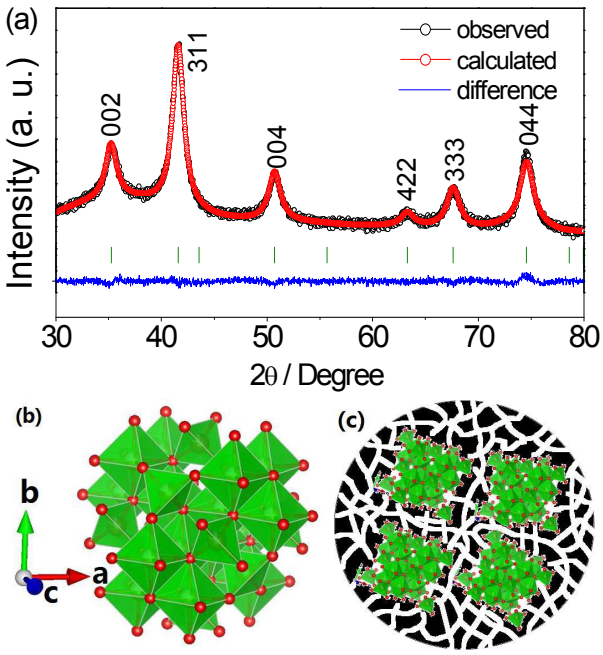

Figure 2 (a) Rietveld refinement of XRD pattern of PC-Fe_3O_4 (R_{wp} = 1.073%, GOF = 1.127). The theoretical Bragg positions were shown with green ticks. (b) Crystalline structure of Fe_3O_4 along c-axis. (c) Schematic structure of PC-Fe_3O_4 composite. Inset green crystallite are Fe_3O_4 nanocrystals, black area are carbon, blank channels are pore channels.

embedded and highly dispersed in the porous carbon. The valence of iron were further confirmed by the XPS. As shown in Figure 3a, the spin-orbit split Fe2p peaks are broad due to a small chemical shift between Fe^{2+} and Fe^{3+}, both of which are present in Fe_3O_4. The Fe^{2+} and Fe^{3+} components were determined by fitting the spectral line shapes to a convolution of Gaussian and Lorentzian functions. The obtained Fe2p2/3 (2p1/2) binding energy is 710.6 eV (725.0 eV) for Fe^{2+} and 711.9 eV (723.6 eV) for Fe^{3+}. These values match the literature

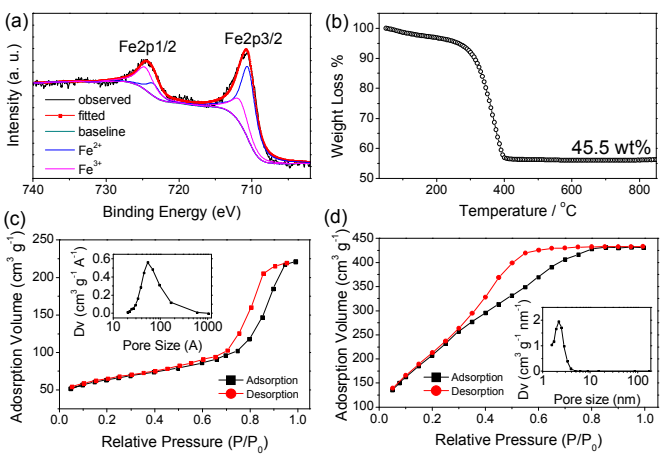

Figure 3 (a) XPS of Fe2p, (b) TGA, and BET analysis of (c) PC-Fe_3O_4 and (d) porous carbon.

values very well.[35-37] The mass percent of Fe_3O_4 was about 44.5% and the surface are of composite could achieve as high as 200 m^2 g^{-1} with porosity around 5.9 nm and rich volume of 0.26 cm^3 g^{-1} (Fig. 3b, c). The rich porosity undoubtedly would be helpful to inhale the electrolyte into the pores for a good transfer ability of lithium or sodium ions.[38]

The reason of introducing oxide of Fe_3O_4 into carbon matrix should be ascribed to the high conductive ability and protection of carbon for Fe_3O_4 in the repeated charge and discharge, as well confirmed in many literatures previously (*e.g.*, Fe_3O_4@C,[39] Fe_3O_4@CF_x[40]). But the contribution of carbon to the capacity of composite was not studied individually before. Herein, we the first time investigated its effect in the sodium ion battery, and an interesting phenomena could be observed. As shown in Figure 4a, a large irreversible capacity existed in the composite of PC-Fe_3O_4, in which a high capacity of 672 mAh g^{-1} was obtained in the 1st cycle but only 252 mAh g^{-1} was delivered in the 2nd cycle. To explore the origin of large irreversible capacity, the electrochemical performance of porous carbon and naked Fe_3O_4 were investigated respectively.

The porous carbon, obtained from the carbonization of resin under the same process, has a very high surface area of 552 m^2 g^{-1}, uniform porosity of 1.9 nm, and rich volume of 0.56 cm^3 g^{-1} (Fig. 3d, Fig. 5a). In the sodium ion battery, it showed a high capacity of 500 mAh g^{-1} in the 1st cycle but delivered a very limited capacity of 10 mAh g^{-1} from the 2nd cycle and even decayed very fast in the following cycles close to 0 mAh g^{-1} (Fig. 5c). By contrast, the irreversibility of the Fe_3O_4 was much smaller (Fig. 5b). Without any carbon modification, the naked Fe_3O_4 particles delivered a capacity of 230 mAh g^{-1} in the 1st cycle and decreased to 130 mAh g^{-1} in the 2nd cycle and then decay gradually to 93 $mAhg^{-1}$ in the initial 50 cycles (Fig. 5d). According to the main peak in the CV around 0.9 V (Inset of Fig. 4a, b), the large irreversibility should be ascribed to the formation of solid electrolyte interface (SEI) on the carbon surface in the first cycle.[41-43] It is clear that the carbon could increase the electronic conductivity and protect the structure of

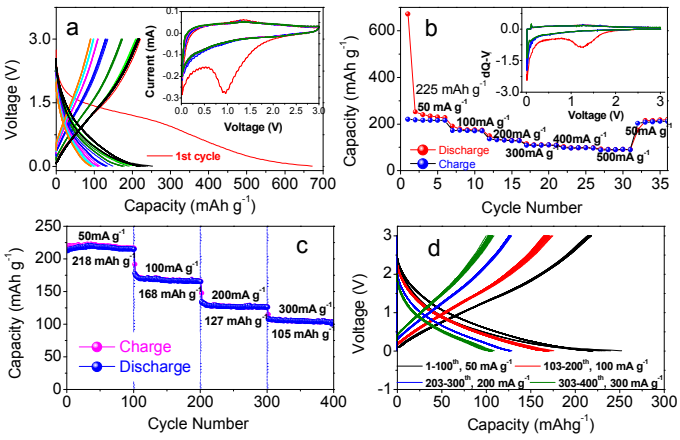

Figure 4 Typical (a, b) rate and (c, d) cycling performance of PC-Fe_3O_4 in sodium ion battery versus sodium metal. Inset of (a) and (b) are CV and dQ-V/V respectively.

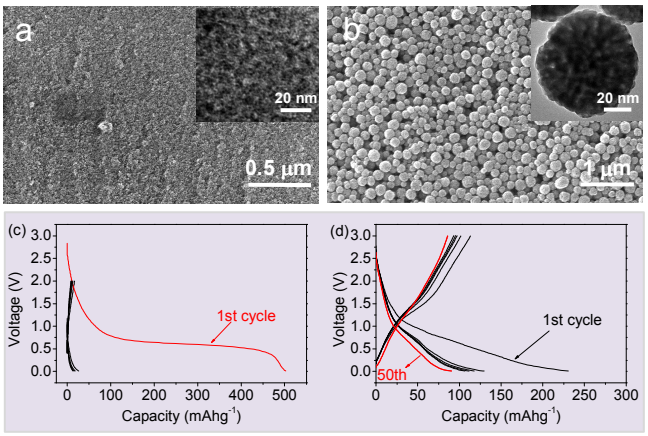

Figure 5 SEM and inset TEM mages of (a) porous carbon and Fe_3O_4 particles. (c) Voltage *vs.* capacity profile of (c) porous carbon and (d) Fe_3O_4 particles obtained by the hydrothermal method.

metal oxide, but it has a very limited capacity contribution in this kind of composite and brings a large irreversibility.

However, compare to the naked Fe_3O_4 particles, the composite of PC-Fe_3O_4 demonstrated higher and stable sodium storage ability. Under the rate test, the average capacities of 225, 168, 127, 103, 98 and 90 $mAhg^{-1}$ could be obtained under the rates of 50, 100, 200, 300, 400 and 500 mA g^{-1}. After the high rate test, the average capacity of the cell could be well recover to 218 mAh g^{-1} at the current density of 50 mA g^{-1} (Fig. 4b). Continually, the cell could still work well with further cycling under the rates of 50, 100, 200, 300 mA g^{-1} more than 400 cycles (Fig. 4c, d). These results well demonstrate the good stability of PC-Fe_3O_4 as electrode, which was mainly ascribed to the protection ability of porous carbon from pulverization. Note that the capacity of PC-Fe_3O_4 was also higher than that of Fe_3O_4-C (< 200 mAh g^{-1}) reported recently.[19] Although the Fe_3O_4 particles obtained by the hydrothermal method have been investigated as anode in the sodium ion battery recently,[19-21] the distinctive advantages of this kind of PC-Fe_3O_4 are the industrial production and equal or even better performance, particularly with a relative low loading of Fe_3O_4 under which the utilization co-efficient of Fe_3O_4 could be largely improved.

To further evaluate the effect of carbon, the composite of Fe_3O_4-C composite with 65wt.% of Fe_3O_4 was also prepared using half amount of resin. But its average capacity of 104 mAh g^{-1} at 100 mA g^{-1} in the initial 50 cycles was much lower than 168 mAh g^{-1} of PC-Fe_3O_4 composite (Fig. 4c, Fig. 6). It should be ascribed to the aggregated Fe_3O_4 within the carbon, which could directly reduce the utilization co-efficient of Fe_3O_4. However, the capacity, coulombic efficiency of 97.5%, and high capacity retention of 90% over 50 cycles (*vs.* the capacity of the 3rd cycles) of Fe_3O_4-C were still much better than naked Fe_3O_4 (*e.g.*, capacity retention of 71.5%) when the 35% carbon introduced in the composite. Note that the reduced capacity of 384 $mAhg^{-1}$ (*vs.* 672 mAh g^{-1} of PC-Fe_3O_4 in Fig. 4a) in the first cycle confirmed again that the irreversible capacity was mainly resulted from the porous carbon due to the low percent

carbon in the composite. In brief, the introduction of carbon could maintain the cycle ability of Fe_3O_4, but an appropriate amount of carbon is necessary to promise its utilization co-efficient.

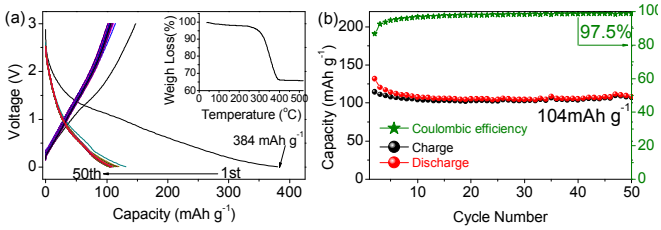

Figure 6 (a) Discharge-charge curves and (b) cycling performances of Fe_3O_4-C composites at 100 mA g^{-1}. Inset of (a) is TGA of Fe_3O_4-C composite with a mass percent of 65wt% Fe_3O_4.

The variation of Fe_3O_4 in the discharge-charge process was characterized by the ex-situ XRD (Fig. 7). The first, the intensity of (004) peak increased after the milling and making an electrode due to the variation of exposed crystal planes, but it is still the Fe_3O_4. It could find that the peaks changes regularly during the discharge and charge based on the reaction of $Fe_3O_4 + 8Na^+ + 8e^- \leftrightarrow 3Fe + 4Na_2O$.[20] Judged from the Fig. 4, the actual capacity of 225 mAh $g_{compoite}^{-1}$ (*e.g.*, 506 mAh g_{Fe3O4}^{-1} versus 44.5wt% of Fe_3O_4 in the PC-Fe_3O_4 composite) was lower than the theoretical value of 926 mAh g_{Fe3O4}^{-1},[20] demonstrating almost half Fe_3O_4 could be reacted with the sodium metal. The electrode after each discharge still show the peaks of Fe_3O_4, which was in good accordance with the capacity as discussed. The increased density of Fe_3O_4 peaks after each charge could be ascribed to the reaction of $3Fe + 4Na_2O \rightarrow Fe_3O_4 + 8Na^+ + 8e^-$, but the peaks of Fe was not obvious (Fig. 7). This phenomenon was very similar as we reported in lithium ion battery recently.[44] But the reversible variations of electrode well confirmed the stability of electrode in the discharge and charge. Bedsides, comparing to the 130 mAh g^{-1} of naked Fe_3O_4, the utilization coefficient of Fe_3O_4 in PC-Fe_3O_4 was 54.6% (*e.g.*, 506 mAhg^{-1} /926 mAh g^{-1}), which

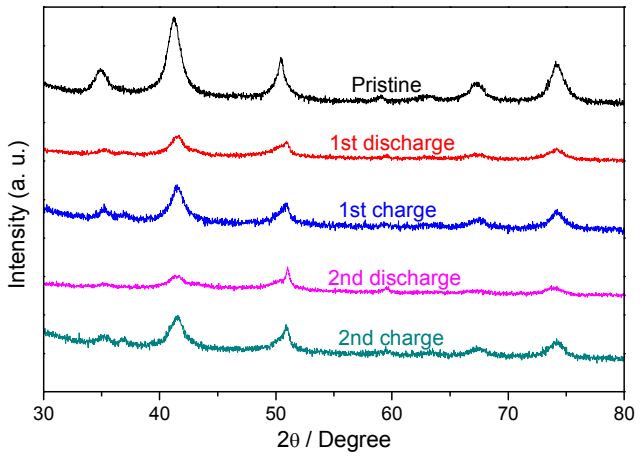

Figure 7 Ex-situ XRD of pristine and cycled electrode.

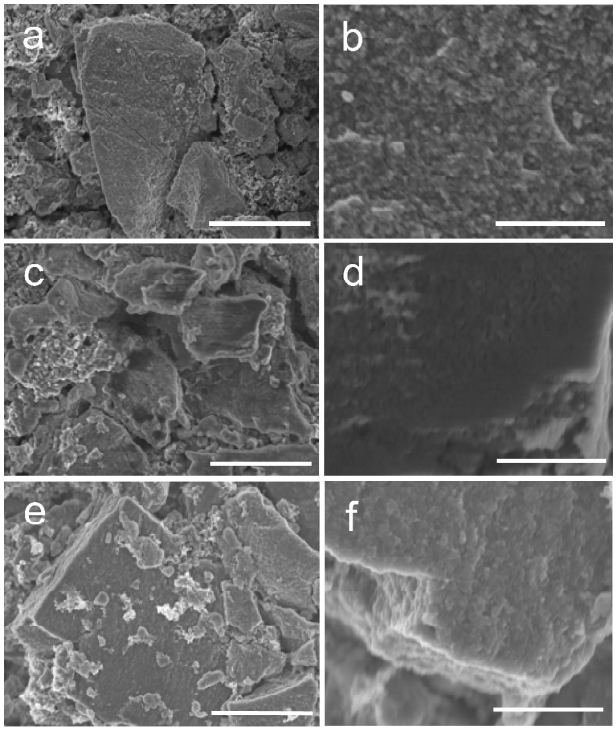

Figure 8 SEM image of (a, b) pristine, discharged and charged electrode in the first cycle with different magnifications. Scale of (a, c, e) and (b, d, f) are 10 μm and 2μm respectively.

was much higher than 14.0% (*e.g.*, 130 mAh g^{-1}/926 mAh g^{-1}) of Fe_3O_4 particles. A high capacity could be obtained with a low amount of Fe_3O_4, and it confirmed that the dispersion of Fe_3O_4 nanocrystals into the porous carbon could largely increase the utilization of metal oxide

Although it is a conversion mechanism with a large volume variation, the stability of electrode well demonstrated the positive effect of carbon to protect the structure in the cycling. Except the proof of XRD, the robust of electrode was further characterized by the SEM. As shown in Fig. 8, the bulky particles of PC-Fe_3O_4 in the electrode were completely preserved after the discharge and charge (Fig. 8a, c, e). After the 1st discharge, we could find that a thick layer of solid electrolyte interface was covered on the pristine PC-Fe_3O_4 particles, making the porous surface become smooth (Fig. 8a-d). The observed SEI resulted from the decomposition of electrolyte and side reactions on the carbon surface of PC-Fe_3O_4 surface, as reported previously.[41] Therefore, it is responsible for the large irreversibility of capacity in the first cycle (Fig. 4a).[45] After the charge process, the smooth layer of SEI and bulky morphology were still preserved, well demonstrating the stability of electrode. As characterized by the TEM (Fig. 1b), the Fe_3O_4 nanocrystals were encapsulated within the porous carbon and then the pulverization of Fe_3O_4 could be largely reduced, thereby obtaining a good cycle ability.

Although $Na_2FeP_2O_7$ has been developed as a new cathode in the sodium ion battery recently,[46-49] it still lacks of example to apply them in the full battery versus metal oxide and investigate

its performance. Herein, we try to introduce it into the sodium ion battery versus the anode of PC-Fe_3O_4. In this way, both anode and cathode are environmental materials and large abundant in the earth, which are critical for maintaining the sustainability in the grid storage. To date, the cathode of layered oxides of P2-type $Na[Ni_{0.25}Fe_{0.5}Mn_{0.25}]O_2$ and NASICON structured $Na_3V_2(PO_4)_3$ have been applied as cathode versus Fe_3O_4-based anode for a full battery,[19,21] but the drawbacks of weak stability of layered oxides and highly toxic of vanadium would inevitably induce the safety problem and limit their practical applications. Considering the strong requirement of sustainability and safety issue in the rechargeable battery, the cathode of $Na_2FeP_2O_7$ was superior than these two kinds of cathode and deserve to be investigated in the sodium ion full battery, particularly versus the PC-Fe_3O_4 which are available to get in an industrial production.

Typical charge-discharge curves of $Na_2Fe_2P_2O_7$ and sodiated PC-Fe_3O_4 were shown in Figure 9. The procedures of designing full battery were similar as reported recently.[40,44,50] Not that the large irreversible capacity of PC-Fe_3O_4 was compensated via the sodiation process, in which the electrode of PC-Fe_3O_4 was sodiated by the sodium metal by the contacting with sodium metal for 30 min, rather than electrochemical compensation.[27] The chemical sodiation process was the same as the lithiation one. The mass ratio of cathode and anode was controlled around 2.32/1 considering their equal of total capacity in battery.[44,50] The average voltage of $Na_2FeP_2O_7$ and PC-Fe_3O_4 were about 2.99 and 0.71 V, and the expected voltage of battery should be around 2.28 V. Via analyzing the work voltage of cathode and anode,[44] the window of work voltage for full battery was about 1.1-4.2V, and the calculated voltage should be around 2.28 V based on the work voltage of cathode and anode (Fig. 9).

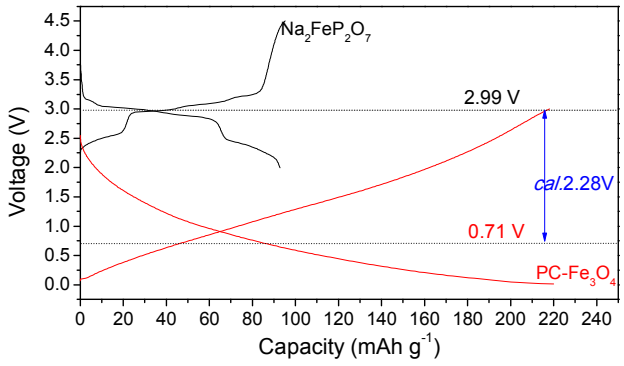

Figure 9 Typical charge-discharge curves of $Na_2FeP_2O_7$ and lithiated PC-Fe_3O_4 composite.

Figure 10 shows the performance of PC-Fe_3O_4/$Na_2FeP_2O_7$ cycled under the rate of 0.1 C. A high capacity of 93 mAh g^{-1} could be obtained with a work voltage of 2.28 V and an energy density of 203 Wh kg^{-1} (which was calculated by the integral of the 1st discharge curve in Fig. 10a). Particularly, the battery could be well cycled over 100 cycles with high capacity retention of 93.3% and a columbic efficiency of 98.5% respectively. And also, the battery has a very excellent rate capability. For example, the capacities of 92, 89, 85, 74, 60, 46 and 32 mAh g^{-1} could be obtained under the rates of 0.1, 0.25, 0.5, 1, 2.5, 5 and 10 C respectively after cycling 20th cycles. It is obvious that such battery has a high rate capability, which should be ascribed to the fast reaction rate of Fe_3O_4 nanocrystals and the fast intercalation/extraction of sodium ion in the stable structure of $Na_2FeP_2O_7$. After the high rate test, the capacity of battery could recover to 90 mAh g^{-1} at the rate of 0.1 C, well demonstrating the stability of electrode. More importantly, the chemical compounds in the reversible reactions of $Fe_3O_4 + Na_2FeP_2O_7 \leftrightarrow NaFeP_2O_7 + Fe + Na_2O$ are low-cost, rich in the earth, environmental-friendly and rather safe. Therefore, this configuration of battery was expected to be widely used in the grid energy, and it could act as energy storage for the conversion of solar and wind energy to the electric power, which was then provided for the individual family conveniently (Fig. 11).

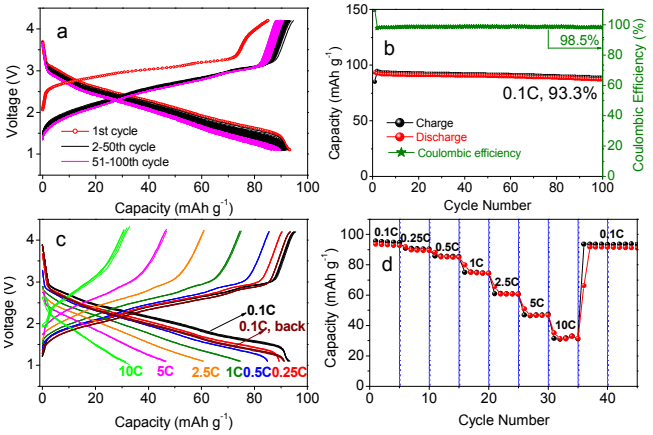

Figure 10 Typical charge-discharge curves and capacity of PC-Fe_3O_4/$Na_2FeP_2O_7$ under (a, b) the rate of 0.1C and (c, d) rate test of 0.1-10C

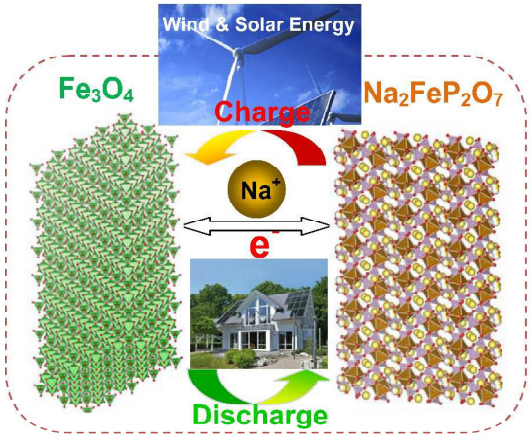

Figure 11 Schematic drawing of iron-based PC-Fe_3O_4/$Na_2FeP_2O_7$ full battery.

Conclusions

One kind of iron oxide-based anode of PC-Fe_3O_4 with a high capacity of 225 mAh g^{-1} at the rate of 50 mA g^{-1} and a stable cycle ability over 400 cycles was introduced in sodium-ion battery for the first time. The production of PC-Fe_3O_4 could achieve an industrial scale towards practical application readily comparing to the traditional Fe_3O_4 particles synthesized by hydrothermal method. Besides, the sodium storage ability, mainly resulted from the conversion of Fe_3O_4 rather than porous carbon, was investigated originally. The stability of electrode was further characterized by ex-situ XRD and SEM. More importantly, a new concept of elemental iron-based sodium ion battery of PC-Fe_3O_4/$Na_2FeP_2O_7$ was presented. This is the first example to introduce an element-rich configuration in sodium ion battery with the viewpoint of sustainability. A superior capacity of 93 mAh g^{-1}, high capacity retention of 93.3% over 100 cycles and work voltage around 2.28 V with energy density of 203 Wh kg^{-1} were well obtained. With the development of batteries in the energy storage, such configuration of iron-based sodium battery would be highly promising and sustainable owing to its low cost, high stability and safety.

Acknowledgment

This work was supported by the Global Frontier R&D Program (2013-073298) on Center for Hybrid Interface Materials (HIM) funded by the Ministry of Science, ICT & Future Planning and the Human Resources Development program grant (No. 20124010203310) of the Korea Institute of Energy Technology Evaluation and Planning (KETEP) funded by the Korean government Ministry of Trade, Industry and Energy. Industry-Academia Cooperation Innovation Fund Projects of Jiangsu Province (Nos. BY2011130) are gratefully acknowledged.

Notes and references

[a]Department of Energy Engineering, Hanyang University, Seoul 133-791, South Korea. Fax: +82 2 2282 7329; Tel: +82 2 2220 0524; E-mail: yksun@hanyang.ac.kr.
[b]College of Chemistry, Chemical Engineering and Materials Science, Soochow University, Suzhou 215123, P. R. China
[c]The Fifth Research Institute of MIIT East China
†These authors contributed equally to this work.

1. J. M. Tarascon and M. Armand, *Nature*, 2001, **414**, 359-367.
2. M. V. Reddy, G. V. S. Rao and B. V. R. Chowdari, *Chem. Rev.*, 2013, **113**, 5364-5457.
3. Y. K. Sun, S.T. Myung, B. C. Park, J. Prakash, I. Belharouak and K. Amine, *Nat. Mater.*, 2009, **8**, 320-324.
4. V. Palomares, P. Serras, I. Villaluenga, K.B. Hueso, J. Carretero-Gonzalez and T. Rojo, *Energ Environ. Sci*., 2012, **5**, 5884-5901.
5. S. Goriparti, E. Miele, F. De Angelis, E. Di Fabrizio, R.P. Zaccaria and C. Capiglia, *J. Power Sources*, 2014, **257**, 421-443.
6. J. Ming, J.B. Park and Y.K. Sun, *ACS Appl Mater Interf*, 2013, **5**, 2133-2136.
7. X. W. Lou, L.A. Archer and Z. C. Yang, *Adv. Mater.*, 2008, **20**, 3987-4019.
8. G. Ji, B. Ding, Y. Ma and J. Y. Lee, *Energy Technol.*, 2013, **2**, 567-572.
9. J. Ming, Y. Wu, J. B. Park, J. K. Lee, F. Zhao and Y. K. Sun, *Nanoscale*, 2013, **5**, 10390.
10. H. L. Zhu, Z. Jia, Y.C. Chen, N. Weadock, J. Y. Wan, O. Vaaland, X. G. Han, T. Li and L. B. Hu, *Nano Lett.*, 2013, **13**, 3093-3100.
11. Y. L. Cao, L.F. Xiao, M.L. Sushko, W. Wang, B. Schwenzer, J. Xiao, Z. M. Nie, L.V. Saraf, Z. G. Yang and J. Liu, *Nano Lett.*, 2012, **12**, 3783-3787.
12. D. Datta, J.W. Li and V.B. Shenoy, *ACS Appl. Mater. Interf.*, 2014, **6**, 1788-1795.
13. L. Wu, X. H. Hu, J. F. Qian, F. Pei, F.Y. Wu, R. J. Mao, X. P. Ai, H. X. Yang and Y. L. Cao, *J. Mater. Chem. A*, 2013, **1**, 7181-7184.
14. Z. Jian, B. Zhao, P. Liu, F. Li, M. Zheng, M. Chen, Y. Shi and H. Zhou, *Chem. Commun.*, 2014, **50**, 1215.
15. S. Yuan, X. L. Huang, D. L. Ma, H. G. Wang, F. Z. Meng and X. B. Zhang, *Adv Mater*, 2014, **26**, 2273.
16. H. Xiong, M. D. Slater, M. Balasubramanian, C. S. Johnson and T. Rajh, *J. Phys.Chem. Lett.*, 2011, **2**, 2560-2565.
17. K. T. Kim, G. Ali, K. Y. Chung, C. S. Yoon, H. Yashiro, Y. K. Sun, J. Lu, K. Amine and S. T. Myung, *Nano Lett.*, 2014, **14**, 416-422.
18. K. J. Harry, D. T. Hallinan, D. Y. Parkinson, A. A. MacDowell and N. P. Balsara, *Nat. Mater.*, 2014, **13**, 69-73.
19. S. M. Oh, S. T. Myung, C. S. Yoon, J. Lu, J. Hassoun, B. Scrosati, K. Amine and Y. K. Sun, *Nano Lett.*, 2014, **14**, 1620-1626.
20. S. Hariharan, K. Saravanan, V. Ramar and P. Balaya, *Phys. Chem. Chem. Phys.*, 2013, **15**, 2945.
21. R. R. Kumar, Y. H. Jung, K. K. Bharathi, C. H. Lim and D. K. Kim, *Electrochim. Acta*, 2014, 146, 503
22. N. Yabuuchi, M. Kajiyama, J. Iwatate, H. Nishikawa, S. Hitomi, R. Okuyama, R. Usui, Y. Yamada and S. Komaba, *Nat. Mater.*, 2012, **11**, 512-517.
23. D. H. Lee, J. Xu and Y. S. Meng, *Phys. Chem. Chem. Phys.*, 2013, **15**, 3304-3312.
24. Z. Liu, Y. Y. Hu, M. T. Dunstan, H. Huo, X. Hao, H. Zou, G. Zhong, Y. Yang and C. P. Grey, *Chem. Mater.*, 2014, **26**, 2513-2521.
25. H. Kim, R. A. Shakoor, C. Park, S.Y. Lim, J. S. Kim, Y. N. Jo, W. Cho, K. Miyasaka, R. Kahraman, Y. Jung and J. W. Choi, *Adv. Funct. Mater.*, 2013, **23**, 1147-1155.
26. P. Barpanda, T. Ye, S. Nishimura, S.C. Chung, Y. Yamada, M. Okubo, H. S. Zhou and A. Yamada, *Electrochem. Commun.*, 2012, **24**, 116-119.
27. I. Hasa, J. Hassoun, Y.K. Sun and B. Scrosati, *ChemPhysChem*, 2014, **15**, 2152-2155.
28. X. Sun and Y. Li, *Angew. Chem. Int. Ed.*, 2004, **43**, 597-601.
29. J. Ming, Y.Q. Wu, G. F. Liang, J.B. Park, F.Y. Zhao and Y. K. Sun, *Green Chem*, 2013, **15**, 2722-2726.
30. H. Kim, R. A. Shakoor, C. Park, S.Y. Lim, J. S. Kim, Y. N. Jo, W. Cho, K. Miyasaka, R. Kahraman, Y. Jung and J. W. Choi, *Adv. Funct. Mater.*, 2013, **23**, 1147-1155.
31. J. Ming, H. Ming, W. J. Kwak, C. Shin, J. Zheng and Y. K. Sun, *Chem. Commun.*, 2014, **50**, 13307-13310.
32. J. Ming, R. Liu, G. Liang, H. Cheng, Y. Yuab and F. Zhao, J. Mater. Chem., 2014, **21**, 10929–10934.

33. N. C. Tombs and H. P. Rooksby, *Acta Crystallogr.* 1951, **4**, 474 – 475.
34. L. B. McCusker, R. B. Von Dreele, D.E. Cox, D. Louer and P. Scardi, *J. Appl. Crystallogr.*, 1999, **32**, 36-50.
35. J. B. Moussy, *J. Phys. D: Appl. Phys.*, 2013, **46**, 143001 (27pp)
36. F. Y. Ran, Y. Tsunemaru, T. Hasegawa, Y. Takeichi, A. Harasawa, K. Yaji, S. Kim and A. Kakizaki, *J. Phys. D: Appl. Phys.*, 2012, **45**, 275002 (5pp)
37. J. Ming, Y. Wu, L. Y. Wang, Y. Yu and F. Zhao, *J. Mater. Chem.*, 2011, **21**, 17776–17782
38. H. Ming, Y. Yan, J. Ming, X. Li, Q. Zhou, H. Huang and J. Zheng, *Rsc Adv*, 2014, **4**, 12971.
39. J. Ming, Y.Q. Wu, G.F. Liang, J.B. Park, F.Y. Zhao and Y.K. Sun, *Green Chem.*, 2013, **15**, 2722-2726.
40. H. Ming, J. Ming, S.-M. Oh, S. Tian, Q. Zhou, H. Huang, Y. K. Sun and J. Zheng, *ACS Appl. Mater. Interf.*, 2014, **6(17)**, 15499-15508.
41. S. Komaba, W. Murata, T. Ishikawa, N. Yabuuchi, T. Ozeki, T. Nakayama, A. Ogata, K. Gotoh and K. Fujiwara, *Adv. Funct. Mater.*, 2011, **21**, 3859-3867.
42. A. Ponrouch, A. R. Goñi and M. R. Palacín, *Electrochem. Commun.*, 2013, **27**, 85-88.
43. K. C. Möller, H. J. Santner, W. Kern, S. Yamaguchi, J. O. Besenhard and M. Winter, *J. Power Sources*, 2003, **119-121**, 561-566.
44. J. Ming, W. J. Kwak, S. J. Youn, H. Ming, J. Hassoun and Y. K. Sun, *Energy Technology*, 2014, **2**, 778-785.
45. M. R. Wagner, P. R. Raimann, A. Trifonova, K. C. Moeller, J. O. Besenhard and M. Winter, *Electrochem. Solid-State Lett.*, 2004, **7**, A201.
46. Y. H. Jung, C. H. Lim, J. H. Kim and D. K. Kim, *Rsc Adv.*, 2014, **4**, 9799-9802.
47. T. Honma, N. Ito, T. Togashi, A. Sato, T. Komatsu, *J. Power Sources* 2013, **227**, 31.
48. C. Y. Chen, K. Matsumoto, T. Nohira, R. Hagiwara, Y. Orikasa and Y. Uchimoto, *J. Power Sources*, 2014, **246**, 783-787.
49. P. Barpanda, G.D. Liu, C. D. Ling, M. Tamaru, M. Avdeev, S. C. Chung, Y. Yamada and A. Yamada, *Chem. Mater.*, 2013, **25**, 3480.
50. H. Ming, J. Ming, S. M. Oh, E. J. Lee, H. Huang, Q. Zhou, J. Zheng and Y. K. Sun, *J. Mater. Chem. A,* 2014, **2**, 18938-18945.

